Available online at www.sciencedirect.com
SCIENCE DIRECT®
International Journal of Heat and Mass Transfer 48 (2005) 4265–4281
International Journal of HEAT and MASS TRANSFER
www.elsevier.com/locate/ijhmt

Mass transfer relations for transpiration evaporation experiments

Hans van Limpt *, Ruud Beerkens, Adriaan Lankhorst, Andries Habraken

TNO Glass Group, P.O. Box 6235, 5600 HE Eindhoven, The Netherlands

Abstract

Transpiration evaporation experiments are often used to study evaporation kinetics from liquids or melts. The mass transport of volatile species in a transpiration experiment depends among others on the flow conditions of the carrier gas in the tube and on the geometrical configuration.

For a transpiration test set-up, CFD modelling showed to be an excellent tool to predict the mass transport of volatile species into a carrier gas and to understand the fluid dynamics in the gas phase and distribution of volatile species in this phase. Relatively simple mass transport relations were obtained for a fixed geometry of the transpiration test set-up. These relations proved to be also applicable for different volatile species and different temperature ranges.

Keywords: Transpiration; Evaporation; Fluid dynamics; Mass transfer

1. Introduction, objective and approach

In many high-temperature melting processes, volatile species evaporate from the surface of the liquid phase into the atmosphere. Some well-known examples are glass melting and metal melting furnaces. Most furnaces exist of a melting tank, charged with raw materials and containing a melt, and a combustion chamber with hot combustion gases.

In current investigations new evaporation models based on mass transfer relations and thermodynamics are developed to predict the evaporation rates of volatile species from different liquids and melts.

Evaporation kinetics is often studied by laboratory scale transpiration tests [1]. The liquid or melt is exposed to an atmosphere of flowing gases (often in a confined space or tube). Temperature, gas flows and gas composition need to be controlled precisely. The mass transfer of volatile species from the liquid phase into the gas atmosphere strongly depends on the flows, the geometry and shape of the gas chamber and the position of the boat with the liquid in this chamber or tube.

Convection and diffusion processes determine the mass transport into the gas phase. Unfortunately, for most reported transpiration evaporation experiments a quantitative description of the mass transport of volatile species into the atmosphere is absent or incomplete. This paper describes a procedure to derive and validate mass transfer relations in transpiration tests for liquids/melts in boats positioned in tube furnaces.

Many mass transfer relations can be derived from literature, but only for relatively simple geometries. For

* Corresponding author. Tel.: +31 40 2650264; fax: +31 40 2650850.
E-mail address: hans.vanlimpt@tno.nl (H. van Limpt).

0017-9310/$ - see front matter © 2005 Elsevier Ltd. All rights reserved.
doi:10.1016/j.ijheatmasstransfer.2005.04.009

Nomenclature

a	chemical activity in melt [–]
A	surface area [m^2]
C	concentration in melt or gas phase [mol m^{-3}]
d	diameter of tube [m]
D	diffusion coefficient [m^2 s^{-1}]
d_{in}	diameter of inner tube in tube-in-tube geometry [m]
H	height of boat [m]
ΔH_{evap}	molar heat of evaporation [J/mol]
h	mass transfer coefficient [m s^{-1}]
h_T	heat transfer coefficient [W m^{-2} K^{-1}]
J	total weight loss [kg]
K, $K(T)$	equilibrium constant [$Pa^{(q-m)}$]
L	length of a boat [m]
L_g	distance from leading edge [m]
l_{in}	length of inner tube or boat in tube-in-tube geometry [m]
l_t	length of tube [m]
m	mass [kg]
p	vapour pressure (Pa)
Q	molar flux density/mass transfer rate [mol m^{-2} s^{-1}]
R	Boltzman gas constant [8.31432 J mol^{-1} K^{-1}]
Re	Reynolds number ($=\rho \cdot v \cdot L/\mu$ or $\rho \cdot v \cdot d/\mu$) [–]
Sc	Schmidt number ($=\mu/\{\rho \cdot D\}$) [–]
Sh	Sherwood number ($=hL/D$ or hd/D) [–]
T	absolute temperature (K)
t	time [s]
v	velocity of gas or melt [m s^{-1}]
W	width of boat [m]
y	distance perpendicular to glass melt surface [m] (vertical direction)
z	distance in gas flow direction [m]

Subscripts and superscripts

*	saturated gaseous atmosphere
avg	average
bulk	parent glass or main gas stream
g	gas phase
h	hydraulic
i	component i in gas phase
in	inner part
j	evaporating component in melt
k	reactive component k in gas phase
m	melt phase
n	normalised conditions (293.15 K and 101325 Pa)
o	outer part
surface	surface of a liquid

Greek and other symbols

μ	dynamic viscosity of fluid phase [Pa s]
δ	Nernst boundary layer thickness [m]
ρ	density [kg m^{-3}]
ϕ	gas flow rate [m^3 s^{-1}]

instance, mass transfer from a flat plat with gas flow in one direction or mass transfer at the inside of a tube or from a sphere [2]. Mass and heat transfer relations for a more complicated set-up or for gas flow with obstructions are rare. In many practical cases, rims or a boat with a liquid disturb the gas flows or gas flows are not well developed above the melt. Therefore it is important to derive mass transfer relations for the transpiration methods and to check their validity.

If the mass transport of volatile species from the liquid into the gaseous atmosphere can be described quantitatively, the transpiration experiments can be used to obtain thermodynamic data like vapour equilibrium pressures and chemical activities of volatile species in the liquid.

1.1. Objective and approach

A quantitative description of the mass transport of volatile species from melts or liquids into the atmosphere is required to derive missing parameters like chemical activities of volatile species and inter-diffusion coefficients of volatile species in the melt or liquid from laboratory transpiration experiments.

The surface of a melt in a large industrial furnace may be considered as an infinite large plate with turbulent or laminar flowing combustion gases along this plate. For transpiration evaporation experiments in a horizontal tube, this assumption is not valid.

In this paper the hydrodynamic behaviour of flowing gases along a boat, positioned in horizontal tubes, is investigated and the results are used to obtain a quantitative mass transfer relation of volatile species into the main gas stream. Important aspects that may influence the mass transfer from a liquid or melt into a gaseous atmosphere are:

- relation between flow rate on the gas velocity profile in the tube and stability of the gas flow;
- the shape and geometrical factors such as shape and size of boat;
- level of filling of the boat.

In order to investigate these aspects, water evaporation experiments in conditioned gas atmospheres were performed in a horizontal tube at room temperature. Water evaporation rates as function of gas flow rate, orientation, position and dimensions of the boat and filling level in boat were determined using an on-line humidity sensor in the gas after passing the boat.

For this investigation also CFD (Computational Fluid Dynamics) calculations were used to solve the equations of change (continuity, motion and mechanical energy) in the system. The results of CFD modelling are compared to the results of simple transpiration evaporation tests with water and acetone as well as to the results of existing empirical mass transport relations that are used to describe the mass transport into the gas phase.

2. Review of mass transfer relations for evaporation processes

As an example of an industrial melting process of a multi-compound liquid with evaporation of different species, glass furnaces are considered shortly. In glass furnaces, evaporation from the liquid surface is one of the main causes of dust and heavy metal emissions. Evaporation of glass melt components will also lead to depletion of volatile glass compounds at the surface layer of the melt (source for cord or silica stones in the glass product) or formation of aggressive vapours (alkali or lead vapours), reacting with the superstructure refractory materials. For some types of glass evaporation results in considerable material losses such as for relatively expensive borates and lead compounds.

The mass transport of the volatile species in the melt, from the bulk to the surface, as well as the mass transport into the gaseous atmosphere is described by an evaporation model, based on mass transfer and thermodynamic relations. The melt or liquid is assumed to be a multi-compound mixture (e.g. slag, glass melt or metal melt). Further on in this paper this multi-compound mixture will be entitled as 'melt'.

Beerkens and van Limpt [3,4] described a model to predict the evaporation rates of volatile species from a glass melt, but the models are based on well-known mass transfer relations derived from literature for relative simple geometrical configurations. The evaporation model describes the evaporation rate for the situation of a static melt in direct contact with flowing gas phases. The model is based on Fick's diffusion law for the melt phase and quasi-steady gas phase mass transfer relations, taking into account changing melt/gas phase boundary concentrations.

By approximation, the evaporation process from melts in industrial melting furnaces can be described as a process of diffusion of a volatile component from the bulk to the surface of an almost static melt (no convection in direction perpendicular to surface) layer moving along the surface of the melt which is exposed to a gas flow or flames over a length L_g, typically a few meters. At the surface of the melt, the component j in the melt reacts or evaporates, forming a volatile component i. This component i diffuses in the boundary layer (1–5 cm thickness) in the gas phase above the melt. Fig. 1 illustrates this process. In cases of static multi-compound melts, depletion of component j at the surface layer of the melt will take place. The degree of depletion depends on time, diffusion rate in the melt and the evaporation rate at the surface.

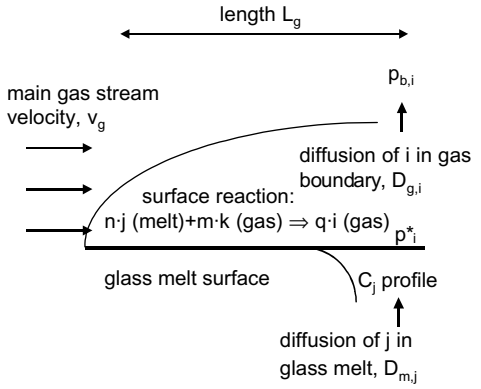

Fig. 1. Schematic presentation of the evaporation process of a component j in a melt released from a melt exposed to a gas flow with a reacting gas species k.

2.1. Mass transport in the gas phase

At the melt surface, at $y = 0$, the loss of component j from the melt is given by

$$Q_{m,j} = -D_{m,j} \cdot \left(\frac{\partial C_j}{\partial y}\right)_{y=0} \quad (1)$$

The molar flux $Q_{g,i}$ of the volatile species i, transported into the gas phase is given by

$$Q_{g,i} = \frac{h_{g,i}}{R \cdot T} \cdot \left(p_i(t)^* - p_i^{bulk}\right) \quad (2)$$

The concentration profile in the melt and the slope: $(\partial C_j/\partial y)_{y=0}$, can be determined by the mathematical solution of the second diffusion law of Fick and Eq. (2). In Eq. (2) $p_i(t)$* is the saturation vapour pressure of volatile specie i. Due to depletion the concentration of volatile melt component j at the surface of the melt as well as the saturation pressure of the volatile gas specie i decrease in time.

The value of the mass transfer coefficient, $h_{g,i}$ depends on the viscosity of the gas, the diffusion coefficient of the volatile specie i in the gas, the velocity of the gas and the position (L_g) downstream the leading edge of the

gas flow parallel to the glass melt surface (L_g = distance from the point where gas flow touches the melt surface).

The local mass transfer coefficient $h_{g,i}$ for mass transport through the boundary layer, adjacent to a flat plate, at the gas phase side at position z (distance) downstream from the leading edge can be estimated by Sherwood relations [2]

$$h_{g,i} = Sh_{g,i} \cdot \frac{D_{g,i}}{z} \tag{3}$$

$Sh_{g,i}$ is the local Sherwood number for gas species i.

The Sherwood number is a function of the Reynolds number (Re), Schmidt number (Sc) and the geometry of the system.

2.2. Heat of evaporation

As a consequence of the evaporation process from a melt or liquid, evaporation enthalpy is withdrawn from the heat contents of a liquid in the boat and consequently the temperature of the liquid will drop. In a stationary situation the temperature of the liquid as well as the heat content of the liquid remain constant. In this stationary situation the temperature of the liquid can be calculated from Eq. (4).

$$Q_{g,i} = \frac{h_T \cdot \Delta T}{\Delta H_{evap}} \tag{4}$$

where h_T is the heat transfer coefficient (in W/m^2/K) from the evaporating specie into the gaseous atmosphere, ΔT the temperature difference between the liquid and the adjacent gas phase in K, ΔH_{evap} the molar heat of evaporation of the volatile specie i in J/mol and $Q_{g,i}$ the evaporation rate of the volatile specie i in mol s^{-1} m^{-2}. As the evaporation rate of specie i increases the temperature difference between the liquid bulk and the gas will rise. However, the liquid surface temperature determines the saturation pressure p_i^* just above the surface and should be known accurately. Due to endothermic evaporation the water surface temperature might decrease and consequently the saturation pressure of $i(p_i^*)$ will become lower than assumed.

3. Transpiration method, experimental set-up and experiments

Several investigators like Conradt [5], Cable and Fernandes [6], Schaeffer and Sanders [7,8] apply laboratory *transpiration* tests to simulate and study the kinetics of the evaporation processes from melts. Such a transpiration set-up often exists of a horizontally positioned ceramic or noble metal tube. The tube is generally heated by electric heating elements. In the horizontal tube, a boat filled with a uniform melt is placed in a section with constant temperature. The melt is exposed to a controlled gas flow. The gas flow rate as well as the gas composition can be adjusted. The evaporation losses are determined, either by measuring the weight losses of the melt or by measuring the gas composition and gas volume flow.

The evaporation rate depends on the vapour pressures and the mass transfer in the gas phase. In case of non-congruent evaporation, the evaporation rate also depends on the diffusion of volatile species in the melt. Vapour pressures are directly related to the chemical activities of the evaporating compounds at the melt surface.

In order to validate the applicability of existing mass transfer relations (Section 4) and CFD calculations (Section 5) for transpiration experiments, transpiration experiments on model liquids with known properties, like water, were performed. Furthermore these experiments were used to obtain qualitative relations between evaporation rates on one hand and different process parameters on the other hand. Process parameters that have impact on the evaporation rates are the gas flow rate, gas flow profile, shape and geometrical aspects of the tube and boat and the height of the rim of the boat.

Two different laboratory set-ups for transpiration evaporation trials were tested and investigated in view of mass transfer kinetics. In the first set-up ('low temperature set-up'), only experiments at room temperature have been performed while in the second set-up (tube furnace) the temperature can be controlled up to 100 °C.

The '*low temperature set-up*' for water and acetone evaporation experiments exists of a transparent inert tube (vitreous silica) with a length of 73 cm and an inner diameter of 6 cm. Fig. 2 schematically shows the set-up. The tube is purged with a controlled volume flow of dry nitrogen (H_2O < 5 ppm) and the gas stream flows along a rectangular boat, partly filled with water. At the outlet a long tube (about 2 m) is connected to ensure that the nitrogen and water vapour are mixed up well. In the outlet of this latter tube a combined humidity/temperature sensor is placed to measure the water vapour concentration and the gas temperature. The sensor, type: Vaisala HMP45A, is calibrated by the manufacturer. All results of this calibration are traceable in terms of dew point to NPL (National Physical Laboratory, United Kingdom) and NIST (National Institute of Standards and Technology, USA) and in terms of temperature to CMA (Finnish National Laboratory for Temperature). To check on possible air leakages the O_2 concentration in the exit gases was measured. Near the inlet of the nitrogen a porous plate is placed to obtain a fully developed laminar gas flow profile in the tube.

The second set-up is a *tube furnace* with a total length of 124 cm (hot zone is 100 cm) and an inner diameter of 10.4 cm. The tube is made of a venerable FeCrAl-alloy. At the tube-inlet, dry nitrogen flushes into the tube and the gas flows along a boat partly filled with water. The outlet of the tube is covered with a flange with two small

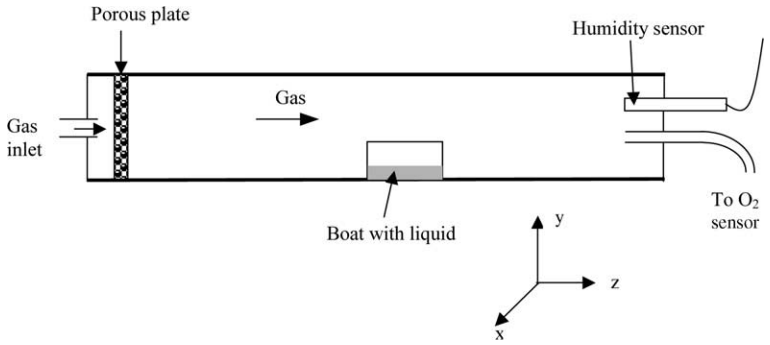

Fig. 2. Schematic presentation of the laboratory test set-up for evaporation experiments at room temperature. The tube is made of vitreous silica, the total length is 73 cm and the inner diameter is 6 cm. In the circular tube different types/shapes of boats can be placed. These boats are partly filled with water or acetone. The porous plate is used to obtain uniform gas flow distribution.

holes. In this second set-up, water evaporation experiments were carried out at room temperature and at a temperature of about 46 °C.

The water evaporation experiments were performed under an atmosphere of pure, dry nitrogen. To describe the mass transport of water vapour from the boat into the atmosphere, the following data on material properties are required:

1. The partial water vapour equilibrium pressure of water ($p^*_{H_2O}$) and acetone ($p^*_{acetone}$) are obtained from data of thermodynamic tables [9,10]. At 20 °C the water vapour equilibrium pressure is about 2336 Pa and the acetone vapour equilibrium pressure is about 32,400 Pa.
2. The diffusion coefficient, D_{H_2O} of water vapour in nitrogen has to be known as a function of temperature at atmospheric pressure. Some values of D_{H_2O} are reported for air as well as nitrogen [11]. The diffusion coefficients can also be estimated from a molecular dynamic approach. Relations for diffusion in binary gas mixtures at low level to moderate level pressures have been described by Chapman and Enskog given by Bird et al. [12] and Reid et al. [11]. Fuller et al. [13–15] described a modified Chapman–Enskog relation for estimating diffusion coefficients in low-pressure binary gas systems with empirical constants based on experimental data. The authors reported an average absolute error of about 4% when using this equation. Based on Fuller's modified Chapman–Enskog relation the diffusion coefficient of water at 20 °C is 2.54×10^{-5} m^2 s^{-1}. Fuller's approach was applied to estimate the diffusion coefficient of acetone into nitrogen. At 20 °C the diffusion coefficient of acetone in nitrogen is $D_{acetone} = 1.1 \times 10^{-5}$ m^2 s^{-1}.
3. For calculation of the Sherwood number, the Reynolds number (Re) and the Schmidt number (Sc) should be determined.

Different experiments were performed to systematically derive the effect of the geometrical configuration, shape of the boat and position of the boat on the transport of water vapour into the atmosphere. The 'low-temperature set-up' was used to determine the impact of the position of the boat in the tube, gas flow rate, filling level of the boat, dimensions of the boat on the evaporation rate of water.

During the experiments with water in the 'low temperature set-up', the nitrogen gas flow is varied between 8.3×10^{-6} and 1.75×10^{-4} m^3_n/s. This means that the Reynolds number (Re) estimated for the tube without obstructions is in the range between 15 and 305. The narrow temperature range is 18–20 °C. In all cases $Re \ll 2300$, which is the critical Reynolds number. Below the critical Re laminar flow conditions are expected.

4. Analytical Sherwood relations

In Section 4.1 the theoretical aspects of analytical Sherwood relations are discussed for different geometries and in Section 4.2 the applicability of these relations is discussed for transpiration experiments with water.

4.1. Theory

Lewis and Whitman [16] described the theory of film models for mass transfer in fluids. This theory describes the mass transfer in a fictive mass transfer boundary layer δ (here the concentration of gas species are position dependent). The conditions of this mass transfer boundary layer (Nernst boundary layer) are

- The mass transfer in the gaseous phase takes place through this boundary layer.
- The mass transfer in this layer only takes place by diffusion.

- The concentration profile is stationary, which means that it is time independent.

Based on these assumptions the equation of continuity in the boundary layer is

$$\frac{d^2C_i}{dy^2} = 0 \tag{5a}$$

Now the boundary conditions are

$$\begin{aligned} &-\text{At } y = 0 \text{ (surface):} \\ &\quad C_i = C_i^* \text{ (equilibrium concentration)} \\ &-\text{At } y = \delta\text{: } C_i = C_i^{\text{bulk}} \end{aligned} \tag{5b}$$

Here C_i is the molar concentration of component i in the gas phase in mol/m^3. As already mentioned in Section 2 the concentration C_i^* is time dependent. From Eqs. (1) and (5a) one can derive

$$Q_{g,i} = \frac{D_{g,i}}{\delta_i} \cdot \left(C_i^* - C_i^{\text{bulk}}\right) \tag{6}$$

and

$$h_{g,i} = \frac{D_{g,i}}{\delta_i} \tag{7}$$

Combining Eqs. (3) and (6) results in the relation between the boundary layer δ and the Sherwood number Sh

$$Sh_i = \frac{z}{\delta_i} \tag{8}$$

For gases, the Sherwood mass transfer relations have analogous Nusselt heat transfer relations [12,17]. For different geometries (e.g. tubes, flat plate) the Nusselt heat transfer relations can be obtained from the VDI-Wärmeatlas [2]. One of the major questions is whether the existing Nusselt heat transfer relations (and Sherwood mass transfer relations) can be used to describe the mass transport of volatile species in transpiration experiments with more complicated shapes and geometrical configurations and with flow obstacles. Possible Sherwood/Nusselt relations that can be used or should be modified for transpiration experiments are:

- Relations for mass transfer at the inside surface of a tube or
- Relations for mass transport between two concentric cylinders.

These relations have to be modified because of the obstruction of the gas flows by the boat and the rim of the boat. The filling level of the boat will also have an influence on the gas flow just above the melt.

Probably, for all laboratory transpiration evaporation experiments the Reynolds number ($Re = \rho \cdot v d/\mu$) for tube flow is lower than about 1000 and this means that laminar flow conditions can be assumed since the critical Reynolds number for gas flows in tubes is about 2500 [18], unless the flows are still not well-developed after a rim or after the inlet tube and still show eddies. Above the critical Reynolds number the transition from laminar to turbulent flow conditions can be expected.

For a tube with a fully developed laminar gas flow without obstacles the average Sh can be obtained from Eq. (9) [2]. The inner diameter of the tube is d, and the length of the tube is l_t. It is assumed that the inner surface of the tube is completely covered by a melt or liquid layer containing a volatile specie j. The average superficial gas velocity in the tube is v_{avg}. Now the Reynolds number is defined as $Re = \rho \cdot v_{avg} \cdot d/\mu$.

$$Sh_1 = 3.66 \quad \text{(asymptotic value for } Sh \text{ in case } Re \cdot Sc \cdot d/l_t \to 0) \tag{9a}$$

$$Sh_2 = 1.615 \cdot \sqrt[3]{\frac{Re \cdot Sc \cdot d}{l_i}} \quad \text{(valid for values of } Re \cdot Sc \cdot d/l_t \gg 0) \tag{9b}$$

$$Sh_{avg} = \{Sh_1^3 + 0.7^3 + [Sh_2 - 0.7]^3\}^{1/3} \quad \text{(valid for } 0 < Re \cdot Sc \cdot d/l_t < \infty) \tag{9c}$$

Gnielinski [19] concluded that the average Nusselt number, obtained from the analogous Eq. (9c) for heat transfer, deviates maximum 1% from the listed numerically calculated average Nusselt number for tubes in the range $0 < Re \cdot Sc \cdot d/l_t < \infty$.

The tube approach can only be used in the case that the liquid/melt surface is assumed to be a part of the inner wall of the tube. In practice a boat with a liquid or melt will be placed in the tube and in that case Sherwood relations derived for two concentric tubes [2,20,21] are expected to improve the prediction of the mass transfer rates. Now the boat in the tube is considered to be shaped cylindrically and placed at the centreline of the tube. The surface of this inner tube is partly covered by a liquid or a melt. This introduces an additional assumption since most boats, and certainly the level of a liquid, are not cylindrically shaper but rectangular. Often the boat is not placed at the centreline and the length of the boat (l_{in}) is much shorter than the length l_t of the tube. The gases flow between the inner and the outer cylinder (or boat).

In this situation d_o is the inner diameter of the outer tube and d_{in} the outer diameter of the inner tube. The hydraulic diameter of the system is defined as $d_h = d_o - d_{in}$ and the Reynolds number is now: $Re = \rho \cdot v_{avg} \cdot d_h/\mu$.

For the theoretical case of Fig. 3(a) and (c), Eqs. (10a)–(10e) can be used to calculate the Sherwood number. It is assumed that radial mass transfer takes places from the inner cylinder to the outer cylinder. The temperature of the whole the set-up and the gas is assumed to be constant.

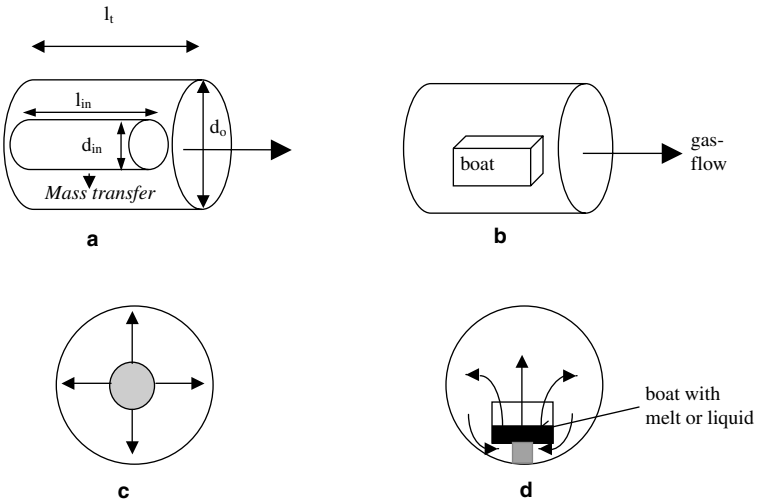

Fig. 3. Schematic presentations of mass transfer in two concentric cylinders from the surface of the inner tube to the inner surface of the outer tube (a + c) and schematic presentations of mass transfer from a boat filled with a melt or liquid to the inner surface of the tube (b + c). (a) Theoretical situation, overviewset-up; (b) practical situation, overview set-up; (c) theoretical situation, cross-section with arrows showing the radial mass transfer from the inner cylinder to the outer cylinder and (d) practical situation; cross-section with arrows showing the mass transfer from the melt in the boat to the outer cylinder.

In case of two concentric cylinders, with a fully developed laminar gas flow and constant concentrations of the volatile species i at the surfaces of both cylinders, Eq. (10a) can be used to calculate the Sherwood number [20,21]. In this situation the concentration profile of component i and the gas velocity profile do not change in the axial-direction.

For situations with a varying concentration profile of component i in the axial direction and a fully developed laminar gas flow, the Sherwood number increases to an asymptotic value for increasing values of $Re \cdot Sc \cdot d_h/l_t$. The Eqs. (10b) and (10c) [20] can be used to calculate the asymptotic value of Sh. Near the inlet of the two concentric cylinders a gas flow profile as well as a concentration profile of the volatile component i are developing. Again, the Sherwood number increases to an asymptotic value for increasing values of $Re \cdot Sc \cdot d_h/l_t$. In this case this asymptotic value of the Sherwood number can be calculated from Eq. (10d) [2].

Now the average Sherwood number for two concentric cylinders with radial transport of component i from the surface of the inner cylinder to the inner surface of the outer cylinder can be calculated from Eq. (10e) [21]. Eq. (10e) can be used in situations in which a gas velocity profile as well as a concentration profile of a volatile component i is developed.

$$Sh_1 = 3.66 + 1.2 \cdot \left(\frac{d_i}{d_o}\right)^{0.5} \tag{10a}$$

$$Sh_2 = f_g \cdot \sqrt[3]{\frac{Re \cdot Sc \cdot d_h}{L}} \tag{10b}$$

$$f_g = 1.615 \cdot \left\{1 + 0.14 \cdot \left(\frac{d_i}{d_o}\right)^{1/3}\right\} \tag{10c}$$

$$Sh_3 = \left\{\frac{2}{1 + 22 \cdot Sc}\right\}^{1/6} \cdot \left(\frac{Re \cdot Sc \cdot d_h}{L}\right)^{0.5} \tag{10d}$$

$$Sh_{avg} = \left(Sh_1^3 + Sh_2^3 + Sh_3^3\right)^{1/3} \tag{10e}$$

4.2. Experimental validation of analytical Sherwood relations

All transpiration experiments discussed in this section were performed in the 'low temperature set-up' (see Fig. 2). The analytical mass transfer relations, discussed in Section 4.1, can only be used in case of laminar flow conditions in the tube. First of all the gas flow conditions were investigated experimentally. Between the positions $49 < z < 56$ cm the measured water evaporation rates seems to be independent of the z-position of the boat in the tube indicating that a fully developed laminar gas flow profile is present in this region. The relation between the different geometrical aspects of boats in the tube and the analytical Sherwood relations also was investigated. The results of these experiments are discussed in the Sections 4.2.1 and 4.2.2.

4.2.1. Evaporation from a water layer at the bottom of a tube

To simulate an experimental situation without a flow obstruction, a water layer is put on the bottom of the tube. The dimensions of this water layer are about

Table 1
Measured and calculated water evaporation rates as a function of the average gas velocity in the tube in case of a water film with a surface area of about 11.5×1.8 cm on the bottom of a tube

Average N_2 gas velocity in tube (m s^{-1})	Measured water evaporation rates (moles/m^2 s^{-1})	Results acc. to Eq. (9)/measured evaporation rates (–)
1.75×10^{-4}	2.58×10^{-3}	0.99
1.50×10^{-4}	2.51×10^{-3}	0.98
1.25×10^{-4}	2.36×10^{-3}	0.98
9.98×10^{-5}	2.22×10^{-3}	0.98
7.49×10^{-5}	2.07×10^{-3}	0.99
6.24×10^{-5}	1.97×10^{-3}	0.98
4.99×10^{-5}	1.85×10^{-3}	1.00
3.75×10^{-5}	1.68×10^{-3}	1.03
2.50×10^{-5}	1.70×10^{-3}	0.95
2.00×10^{-5}	1.91×10^{-3}	0.80
1.50×10^{-5}	1.87×10^{-3}	0.78
1.00×10^{-5}	1.67×10^{-3}	0.80

For the calculations the Sherwood relations for mass transfer in radial direction from the inner surface of a tube geometry have been used (Eq. (10)). The water vapour bulk concentrations are calculated for each volume ΔV part of the tube.

11.5×1.8 cm ($L \times W$). The thickness is only 1–2 mm. The hydraulic diameter of the tube with the water layer is 5.8 cm.

Table 1 shows the measured evaporation rates as a function of the average gas velocity in the tube as well as the calculated evaporation rates according to Eq. (9). For average gas velocities $\geqslant 2.5 \times 10^{-5}$ m s^{-1} the results of the measurements and calculations deviate less than 5%. For lower gas velocities the water vapour pressure in the main gas stream ($p^{\text{bulk}}_{H_2O}$) will increase and for the modelling it becomes more important to know the local water vapour in the main gas stream accurately (see Eq. (2)).

4.2.2. Impact of filling level of the boat on the water evaporation rate

Using a rectangular boat of $4.7 \times 2.2 \times 1.8$ cm ($L \times W \times H$), different water evaporation tests were performed. The level of water in the boat was changed for the different experiments. By decreasing the amount of water, the height of the rim above the liquid of the boat increases (see Fig. 4)

$$h_{\text{rim}}\ (\text{cm}) = 1.8 - 0.1 \cdot m_{H_2O} \tag{11}$$

In this formula h_{rim} is the height of the rim above the water surface in cm and m_{H_2O} is the mass of the water in the boat in gram. It is assumed that the density of the water is 1.0 kg/m^3. The measured water evaporation rates increased when increasing the water level. For low amounts of water $\leqslant 2.5$ g ($1.55 \leqslant h_{\text{rim}} < 1.8$ cm), the obtained relations between the gas flow rate and the measured evaporation rates are about the same. However, in case the boat is almost completely filled, an increase of the amount of water in the boat from 18 to 19 g shows a significant impact on the evaporation rate. In case of 19 g water in the boat the water surface bellies out due to the high surface tension of water and the height of the water surface exceeds the height of the side walls about 0.1 cm.

As can be seen in Fig. 5, for all filling levels nearly linear relations were found between the reciprocal gas velocity and the measured water vapour pressures.

4.3. Discussion analytical Sherwood relations

The measured evaporation rates from experiments with a water layer at the bottom of a tube seem to correspond rather well with results obtained from the Sherwood mass transfer relations for radially directed mass transport inside a tube (Eq. (9)). In this set-up the gas velocity profile in the tube will hardly be disturbed. In Table 1 the measured evaporation rates as well as the results of the calculations according to the Sherwood relations for inner tube surfaces (Eq. (9)) are shown. The water layer at the bottom of the tube can be considered as a part of the inner tube wall. Eqs. (2) and (3) are used to calculate the molar transport of water vapour into the main gas stream in this tube. For the simulation, the water vapour pressure in the main gas stream ($p^{\text{bulk}}_{H_2O}$) increases as the flow passes the water surface. To calculate the partial vapour pressure of water vapour in the main

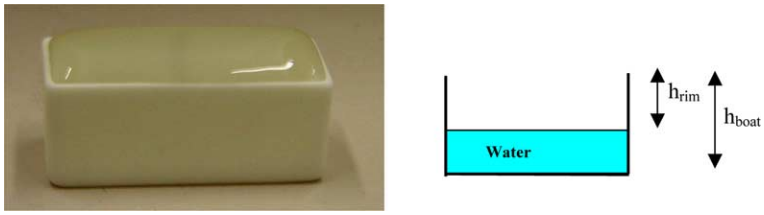

Fig. 4. Rectangular boat used for water transpiration tests with different amounts of water in the boat. Because of the various amounts of water the height of the rim varies. The picture shows the boat filled with 19 g of water. The water surface layer exceeds the height of the sidewalls by about 0.1 cm.

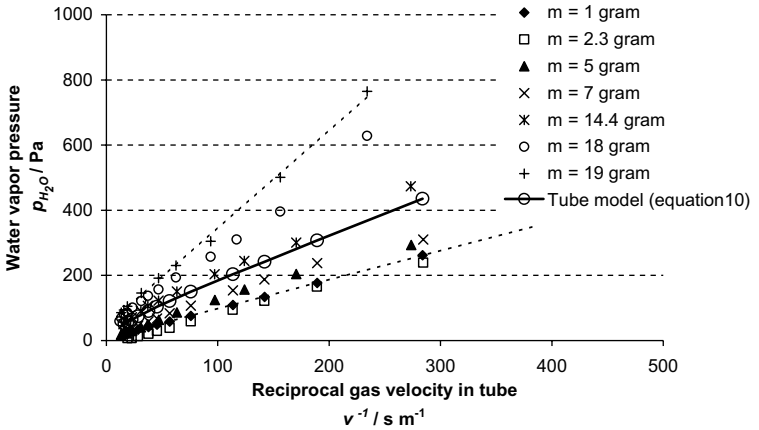

Fig. 5. Measured water vapour concentrations in exit as a function of the reciprocal gas flow rate and the amount of water in the boat.

gas stream ($p^{\text{bulk}}_{H_2O}$), the interface water–gas in the mass transfer model is divided in the z-direction into n parts with each a length Δz and volume $\Delta V(\Delta V = \pi \cdot d_h^2 \cdot \Delta z/4)$. For each volume part ΔV of the tube, the mass conservation equation has been applied to calculate the local bulk concentration of water vapour in the gas phase and gas velocity. In all cases perfect mixing of all gaseous species within the volume elements is assumed.

Since the measured water vapour pressures will always be below the equilibrium vapour pressure at room temperature (about 2200 Pa) the contribution of the water vapour to the total gas flow (gas velocity) will be less than 0.22% and is neglected for all water transpiration experiments at room temperature.

Simple Sherwood relations for mass transfer inside tubes without any obstruction cannot be used to describe the results of the water evaporation experiments with boats partly filled with water (Section 4.2.2). Fig. 5 shows the calculated water vapour pressures obtained from Eq. (9). At the position of the boat the hydraulic diameter of the tube is assumed to be 5.5 cm and the water vapour pressure in the main gas stream ($p^{\text{bulk}}_{H_2O}$) is assumed to be nil.

The measured water evaporation rates are significantly affected by the height of the rim of the boat. For the situation the boat is *completely filled* there is no rim (see Fig. 4) and from the leading edge a gas flow profile as well as a concentration profile is developed. The Sherwood relation for two concentric tubes (Eq. (10e)) probably improves the prediction of the mass transfer rates from a completely filled boat with water in the tube. The boat inside the tube is assumed to be cylindrically shaped and the water surface is a part of the outer surface of this cylinder. Radial mass transfer takes place from the water surface to the inner surface of the tube. The hydraulic diameter of the completely filled rectangular boat (the virtual inner tube) is calculated by using the definition of hydraulic diameter [18]: four times the area of the surface of the boat perpendicular to the flow direction divided by the circumference of this surface: $d_h = 4 \times 1.98 \times 2.47/8.9 = 2.20$ cm.

The Sherwood relation for two concentric cylinders (Eq. (10e)) was also applied to predict the radial mass transfer for two rectangular boats placed in series and an elongated boat. In all cases the boats were completely filled with water. In Fig. 6 the results of the measurements are compared to the predicted results based on the mass transfer equation (10e) and the calculated vapour pressures were in good agreement with the measured vapour pressure.

5. Numerical solutions of mass transport phenomena

The mass transfer of volatile species during the transpiration experiments, as described in the previous section, only can be calculated from Eqs. (9) and (10) for well-defined conditions and for relatively simple geometrical configurations. For more complex geometries and in gas flows with obstructions the mass transport problem has to be solved numerically. For these situations numerical CFD (Computational Fluid Dynamics) models have to be used, which solve the equations of change (continuity, momentum and mass transport) within the system.

5.1. Theory

In our work the software package GTM-X is used to perform these CFD simulations. GTM-X is a CFD-model developed by TNO and specially designed to simulate glass melt processes. GTM-X is a flexible code capable of both steady-state and time-dependent simulations. The code is block-structured. Per domain different sets of models can be selected (e.g. there is no need to solve

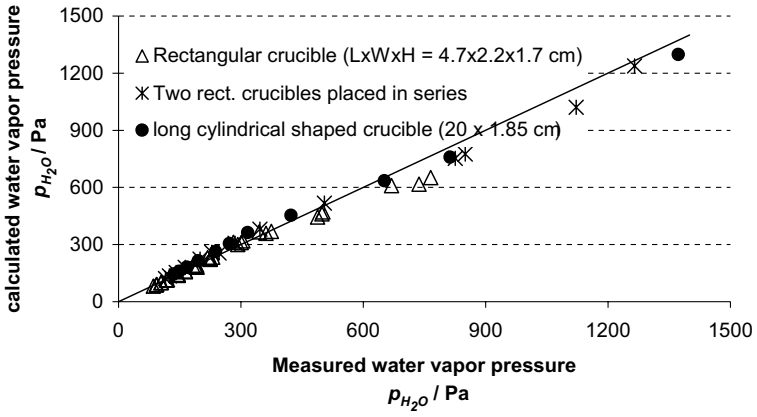

Fig. 6. For three different shaped boats positioned in a cylindrical tube the measured water vapour concentrations are compared to the results of mass transfer Eq. (10e) for two concentric cylinders assuming radial mass transport from the water surface to the inner surface of the tube. All boats were completely filled with water.

for flow in refractories or for turbulence in the glass bath), allowing differentiation of the equations that are solved for on each block, saving valuable CPU-time. Per block, the body-fitted grid is structured and within each block the level of grid refinement can be specified, enabling the use of many grid cells and accurate discretization only where it is really needed. Details on the physical models and numerical methods that have been used in GTM-X can be found in Batchelor [22], Ferziger and Perić [23] and Patankar [24]. Furthermore, GTM-X has been parallelised so that a computation can run simultaneously on several computers, thus further reducing the CPU-time [25,26].

5.1.1. Governing equations

The stationary gas flow pattern and the volatile species concentration distribution in the tube are calculated in three dimensions. The flow rate in the tube (Reynolds number) is low ensuring that the flow remains in the laminar flow regime. The governing equations for stationary laminar flow with species mass transport in three dimensions can be found in e.g. Bird et al. [12]. The mass conservation equation, or mass continuity equation, for an incompressible fluid with constant density reads

$$\frac{\partial v_x}{\partial x}+\frac{\partial v_y}{\partial y}+\frac{\partial v_z}{\partial z}=0 \tag{12}$$

Assuming that the viscosity is constant, the momentum equations—or Navier–Stokes equations—for the velocities in three directions read

$$\rho\left(v_x\frac{\partial v_x}{\partial x}+v_y\frac{\partial v_x}{\partial y}+v_z\frac{\partial v_x}{\partial z}\right)=-\frac{\partial p}{\partial x}+\mu\left(\frac{\partial^2 v_x}{\partial x^2}+\frac{\partial^2 v_x}{\partial y^2}+\frac{\partial^2 v_x}{\partial z^2}\right) \tag{13}$$

$$\rho\left(v_x\frac{\partial v_y}{\partial x}+v_y\frac{\partial v_y}{\partial y}+v_z\frac{\partial v_y}{\partial z}\right)=-\frac{\partial p}{\partial y}+\mu\left(\frac{\partial^2 v_y}{\partial x^2}+\frac{\partial^2 v_y}{\partial y^2}+\frac{\partial^2 v_y}{\partial z^2}\right) \tag{14}$$

$$\rho\left(v_x\frac{\partial v_z}{\partial x}+v_y\frac{\partial v_z}{\partial y}+v_z\frac{\partial v_z}{\partial z}\right)=-\frac{\partial p}{\partial z}+\mu\left(\frac{\partial^2 v_z}{\partial x^2}+\frac{\partial^2 v_z}{\partial y^2}+\frac{\partial^2 v_z}{\partial z^2}\right) \tag{15}$$

The conservation equation for the mass fraction C of volatile species with constant diffusion coefficient reads

$$v_x\frac{\partial C}{\partial x}+v_y\frac{\partial C}{\partial y}+v_z\frac{\partial C}{\partial z}=D_{g,i}\left(\frac{\partial^2 C}{\partial x^2}+\frac{\partial^2 C}{\partial y^2}+\frac{\partial^2 C}{\partial z^2}\right) \tag{16}$$

where, ρ is the density, v the dynamic viscosity and $D_{g,i}$ the diffusion coefficient.

It is assumed that there is no significant heat exchange of the tube with the ambient and that the gas flow is in thermal equilibrium with the tube and liquid container. Also, any thermal effects due to evaporation are neglected, which certainly is true for the lower flow rates. Thus, the temperature of the whole system is assumed to be uniform and no separate energy equation needs to be solved. The five transport Eqs. (12)–(16) are computed iteratively, based on the finite volume method according to Patankar [24].

5.1.2. Boundary conditions

The boundary conditions of the system are:

- At the inlet of the tube ($z = 0$) the concentration of the volatile species $C_i = 0$ and a fully developed laminar gas flow velocity profile is assumed, with an average v_z-velocity according to the applied mass flow;

- On the evaporating surface of the liquid in the container, at the liquid–gas interface just in the gas phase, the vapour pressure is in equilibrium with the liquid: $C_i = C_{i.}^*$;
- On all solid boundaries (tube and container walls), the three velocity components are set to zero and for the volatile species, a zero mass flux is applied (no condensation or evaporation);
- On the outflow boundary, the gradient for both the volatile species and the normal velocity component are set to zero, whereas the tangential velocity components are set to zero.

5.1.3. Geometry and grid point distribution

Throughout the flow domain within the tube, a mesh or grid of volume cells has been constructed (see Fig. 7). On each of these volume cells the above-defined set of differential equations is discretized. Three velocity components, pressure and the concentration of the volatile species are calculated in each cell or node. A total number of 1.6×10^5grid nodes have been used.

5.2. Results CFD modelling

The results of the water evaporation tests are compared to the results of CFD modelling. CFD modelling is used to calculate the gas velocity profiles as well as the concentration profiles of the water vapour in the tube. Based on the average water vapour concentration and the average gas flow at the outlet of the tube, the total amount of released water vapour was calculated.

The first simulation is performed for a rectangular Al_2O_3 boat ($L \times W \times H = 4.7 \times 2.2 \times 1.8$ cm) placed in a tube with an inner diameter of 6 cm (see Fig. 2). The boat is filled with 7 g water and the height of the rim above the liquid surface is 1.1 cm. For a flow of 1.4×10^{-5} m_n^3/s the gas flow profiles in and above the boat are shown in Fig. 8(A) and (B). Near the sidewalls of the boat above the surface of the liquid, recirculation areas are observed. The maximum gas velocity in the boat is observed near the centre of the crucible in the same direction as the main gas stream. At much higher gas flow rate of 2.2×10^{-4} m_n^3/s, the recirculation loop is found to completely occupy the area above the water surface (see Fig. 8C). For the last situation, with the relatively high gas flow rate, the flow direction just above the water surface is opposite to the direction of the main gas stream and the gas velocity just above the water surface increases in the upstream direction of the main gas flow.

For the experiment with a gas flow of 1.4×10^{-5} m_n^3/s, the calculated water vapour concentrations above the water surface are given in Fig. 9A. Downstream of the leading edge of the boat the thickness of the Nernst boundary layer increases and consequently the local water evaporation rate decreases with downstream distance from the leading edge (see Eq. (6)). However, for a gas flow of 2.2×10^{-4} m_n^3/s the gas flow direction in the boat is reversed and near the leading edge the lowest evaporation rates were observed (see Fig. 9(B)). For three different points above the water surface the water vapour concentrations are given as a function of the height above the water surface (Fig. 10). In this situation the thickness of the Nernst boundary layer can be calculated from the slope $(dc/dy)_{y=0}$. The Nernst boundary layer varies from about 2.6 cm near the leading edge to 0.9 cm at the opposite side of the boat.

The measured average water vapour concentrations in the exiting gas flow are compared to the values obtained from the CFD modelling. Fig. 11 shows the water vapour concentration as a function of the average Reynolds number in the tube. Excellent agreement between simulations and measurements is found as measured water vapour concentrations are maximum 2% lower than the modelled water vapour concentrations over the complete range of Reynolds numbers. Differences between simulations and experiments, especially

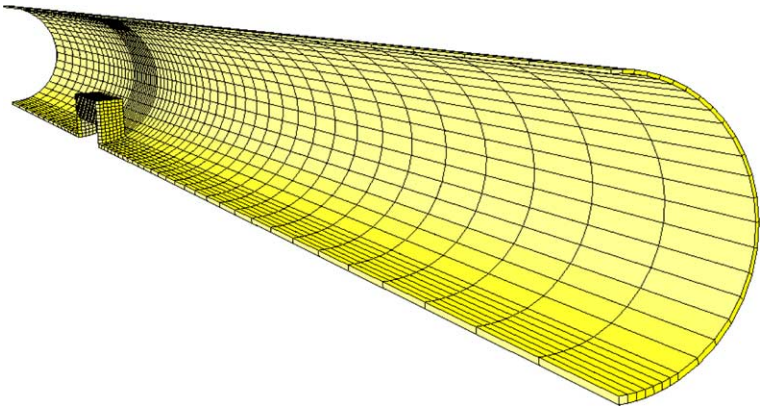

Fig. 7. Geometry of the tube and the grid point distribution projected on the tube wall and on the liquid-filled container.

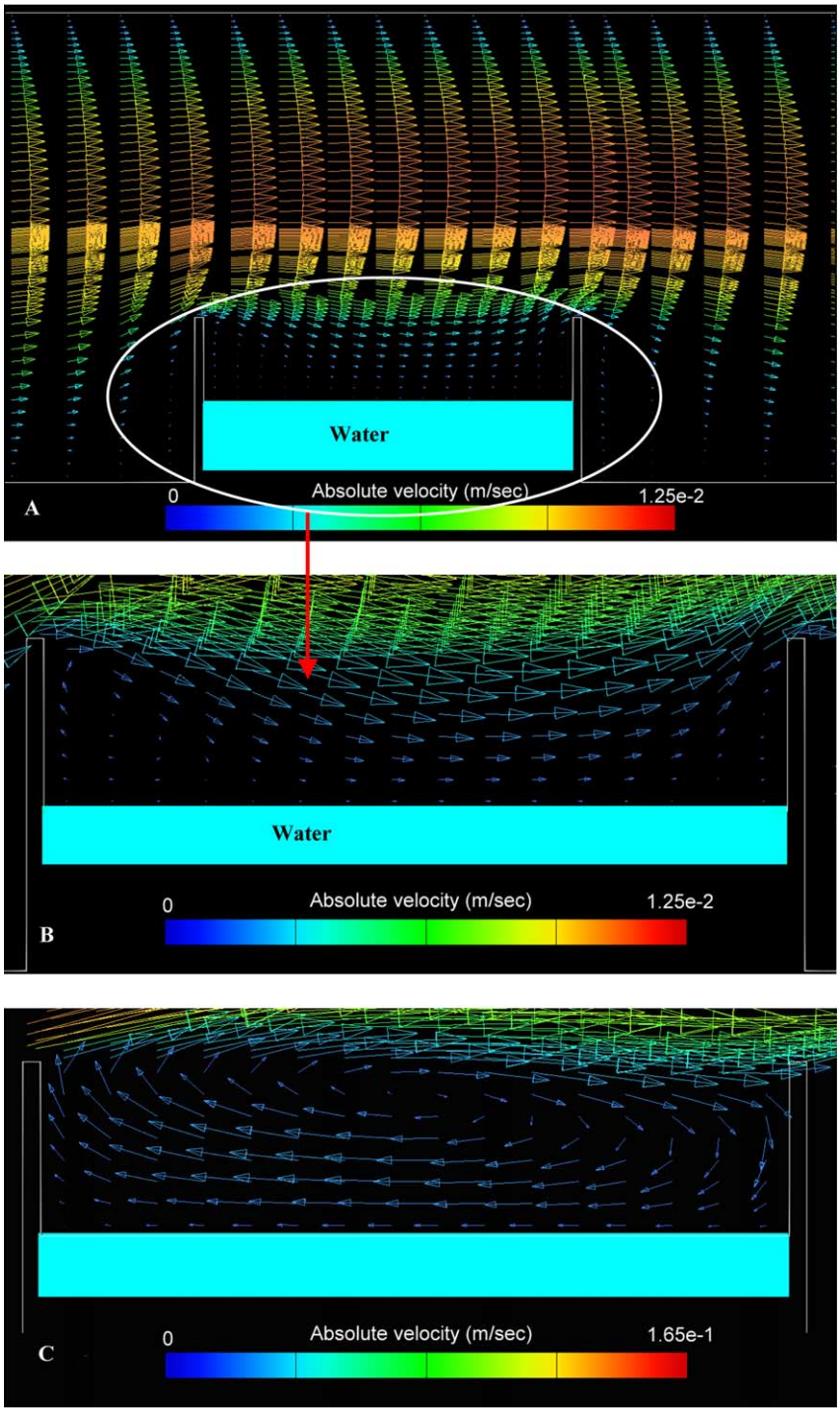

Fig. 8. Calculated gas velocities derived from CFD modeling of a transpiration experiment with a rectangular boat ($L \times W \times H = 4.7 \times 2.2 \times 1.8$ cm) filled with 7 g water. The figure shows the gas velocity vectors in the tube and the free space of the boat. The height of the rim above the water surface is 1.1 cm and the diameter of the tube is 6 cm. In (A) and (B) the N_2 average gas velocity in the tube is 0.5 cm s^{-1} and in (C) the average gas velocity is 7.7 cm s^{-1}. The temperature is assumed to be constant 20 °C.

at higher flow rates, can be attributed to the fact that in the modelling study a homogenous temperature-profile is assumed and the heat of evaporation is not taken into account as will be shown below.

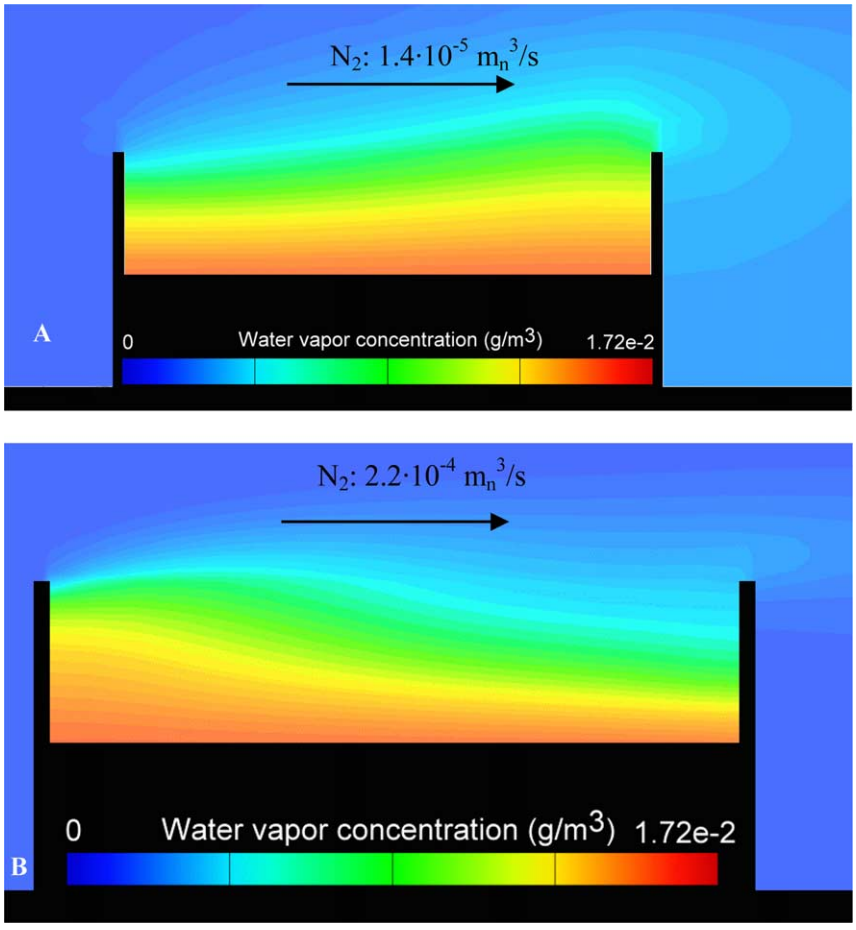

Fig. 9. Results CFD modeling for transpiration experiment with a rectangular boat ($L \times W \times H = 4.7 \times 2.2 \times 1.8$ cm) filled with 7 g water. The gas flow rate was: (A) 1.4×10^{-5} m_n^3/s and (B) 2.2×10^{-4} m_n^3/s. The figure shows the water vapour concentrations just above the water surface in g/m^3.

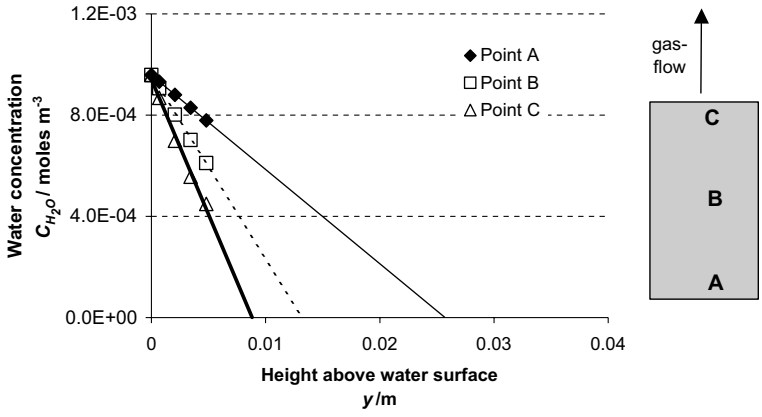

Fig. 10. From Fig. 9 calculated water concentration profiles for three points (A, B and C) above the water surface.

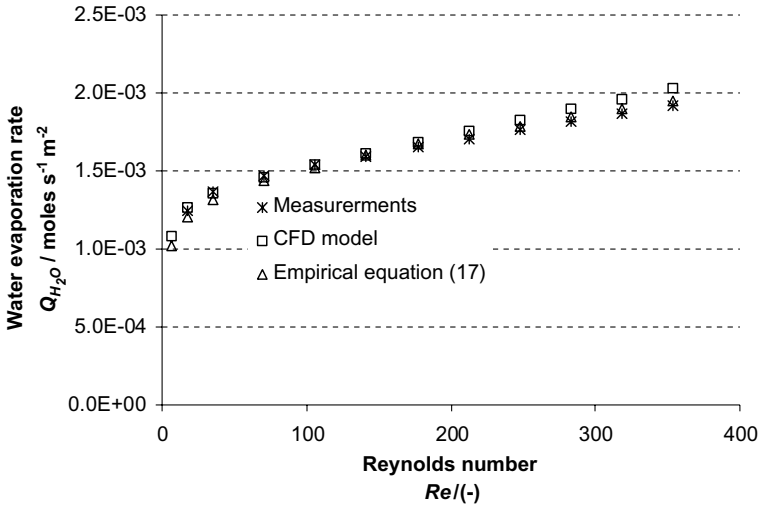

Fig. 11. Measured and predicted water evaporation rates from a rectangular boat ($L \times W \times H = 4.7 \times 2.2 \times 1.8$ cm) filled with 7 g water. The tests were done in the 'low-temperature set-up' at room temperature.

5.2.1. Heat of evaporation

During a transpiration experiment with water, the temperature profile near the water surface was measured with a thermocouple. The N_2 gas flow was 1.25×10^{-4} m_n^3/s, the gas temperature is set on 18.6 °C and the measured water evaporation rate was 3.7×10^{-3} mol s^{-1} m^{-2}.

During the evaporation experiment the temperature of the water bulk lowered to 14.2 °C. However, within 4 mm above the water surface the temperature of the gases rose to 18 °C. The diameter of the thermocouple is 1 mm and the vertical position of the thermocouple can be determined with an accuracy of about 1 mm. Accurate measurements of the water surface are not possible with a thermocouple because of the physical contact between the thermocouple and the water surface. As soon as the thermocouple touches the water surface a rim of water covers the tip of the thermocouple due to the high surface tension of water. The temperature decrease near the water surface influences the gas properties such as density, viscosity and diffusivity, thus slightly modifies the mass transfer rate.

6. Empirical mass transfer relations for transpiration experiments

Basically, the CFD models are used to predict the mass transport in the gas phase for rather complex geometries and shapes, like transpiration set-ups with rectangular, partly filled boats in horizontal cylindrical tubes. The CFD modelling and relatively simple water evaporation experiments have been performed to find or test mass transfer relations, describing the kinetics of evaporation in transpiration experiments and to validate these relations or to simplify relations. Such relations are required for scaling up transpiration methods to industrial furnaces or to derive vapour pressures or diffusion coefficients from results of transpiration tests.

6.1. Theory

For flat plates [2] and tube geometries the Sherwood number is proportional to $Sc^{1/3}$ (Eq. (9b)). However, the mass transfer equations between two concentric cylinders (Eqs. (10a)–(10e)), will probably give a better explanation of the experimental results from the transpiration experiments with a rectangular boat in a tube. A fitting procedure based on the general equation given by Eq. (17) is used to describe the relation between *Sh*, *Re* and *Sc*.

$$Sh^3 = C_1 + C_2 \cdot Re \cdot Sc + \left(\frac{2}{1 + 22 \cdot Sc}\right)^{0.5} \cdot C_3 \cdot (Re \cdot Sc)^{1.5} \quad (17)$$

In Section 6.2 transpiration experiments with water and acetone are discussed to validate this empirical relation.

6.2. Validation of empirical mass transfer relations for transpiration experiments

Based on these water evaporation experiments and the CFD modelling a general analytical Eq. (17) involving the parameters: *Re* and *Sc* was derived, in order to predict Sherwood numbers for different volatile species, gas compositions, temperature levels and gas flows. In

first instance independent evaporation experiments with acetone under a nitrogen atmosphere were performed using the 'low-temperature set-up' and secondly water evaporation experiments at higher temperatures (about 46 °C) were carried out. In the tube furnace the maximum Reynolds-number in the undisturbed flow is about 1000 ensuring laminar flow conditions.

6.2.1. Water and acetone transpiration experiments

The experiments were done with water and acetone at room temperature and the filling levels in the boat are always the same. For all experiments the same carrier gas was used (N_2). The nitrogen gas flow rate was controlled at a value within the range 1.0×10^{-5} and 2.0×10^{-4} m_n^3/s and the height of the rim above the liquid surface was 1.1 cm. Based on the water evaporation experiments, the values for the constants C_1, C_2 and C_3 in Eq. (17) were obtained. For the same geometrical configuration these values should be constant and should not depend on gas flow, temperature and type of liquid. Now Eqs. (2) and (3) were used to predict the evaporation rates of acetone. Fig. 12 shows the predicted evaporation rates, according to Eq. (17), versus the measured evaporation rates. In these calculations the bulk concentration, C_i^{bulk}, is assumed to be the average concentration of component i in the outlet of the tube

$$C_i^{\text{bulk}} = Q_i \cdot A/\phi_{\text{avg}}.$$

where A is the area of the surface of the liquid in the boat (in m^2) and ϕ_{avg} is the average gas flow rate in the tube (in $m^3\,s^{-1}$). According to the least squares method the average error in the predicted water vapour evaporation rates is 0.9% and the error in the predicted acetone evaporation rates is 2.6% using $C_1 = 43.0$, $C_2 = 0.454$, $C_3 = 5.1.10^{-3}$.

In Fig. 11 the experimental results from the transpiration tests, the results of the CFD modelling and the obtained results from Eq. (17) for the water vapour evaporation tests were plotted versus the Reynolds number in the tube (all for the same experimental configuration). Accurate measurements were not possible for $Re < 17$ and therefore in this range only the results of the CFD models are compared with the results from the application of the empirical relation 17. However, even in the range: $7 < Re < 17$, the results deviate less than about 6%. In the range: $17 < Re < 354$, the average error is even less than 0.5%.

Additional water transpiration experiments have been performed in a tube furnace (see chapter 4) to test the validity of Eq. (17) also for another experimental set-up and another situation. Again the same rectangular Al_2O_3 boats were used and filled with 7 g of water. The tube was flushed with dry nitrogen and experiments were carried out at room temperature (about 18 till 19 °C) and a temperature of about 47 ± 1 °C. The Reynolds numbers of the laminar undisturbed gas flow was controlled at a value in the range between 4 and 1026. The evaporation losses have been determined by measuring the weight losses of the boats after the transpiration experiment. The results are shown in Fig. 12. The experimental results at room temperature and Eq. (17) were used to derive the values of C_1, C_2 and C_3 for this set-up and to predict the water evaporation rates at 47 °C. The average error in the predicted water

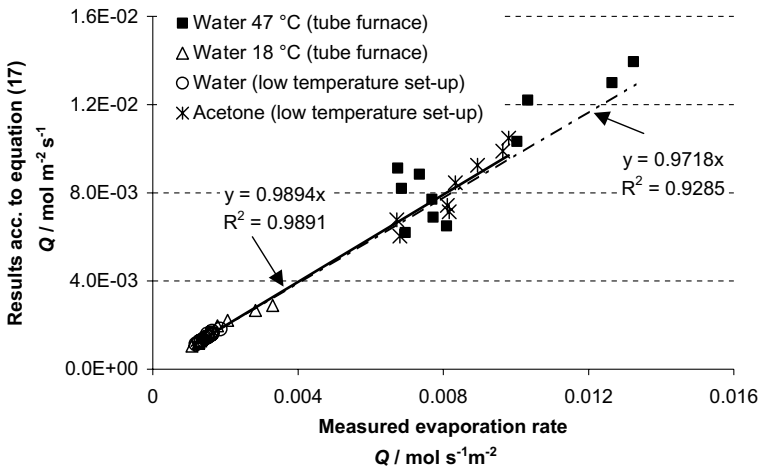

Fig. 12. Predicted evaporation rates versus measured evaporation rates of water and acetone using Eq. (17) to predict the average Sherwood number. For the water and acetone evaporation tests performed in the 'room temperature set-up' the values for the constants are: $C_1 = 43.0$, $C_2 = 0.454$ and $C_3 = 5.1 \times 10^{-3}$. For the water evaporation tests in the tube furnace, the measurements at room temperature were used to obtain numerical values for the constants: $C_1 = 196.6$, $C_2 = 0$ and $C_3 = 0.397$. The tube furnace was flushed with dry N_2 and the Reynolds number of the undisturbed gas flow varied between 7 and 1026.

evaporation rates compared to the experimentally found evaporation rates at 47 °C is about 4.8% according.

7. Conclusions

The mass transport of volatile species during a transpiration experiment depends among others on the flow conditions of the carrier gas in the tube and on the geometrical configuration of the transpiration set-up (shape, size and position of boat and filling level with liquid). Based on the results of this paper it is concluded that the gas flow profile in the tube, the position and dimensions of the tube as well as the filling level of the boat have a large influence on the mass transfer of volatile species into the gaseous atmosphere.

In most glass melt evaporation studies no mass transfer relations for transpiration experiments are available. This paper shows that Sherwood relations for a specific geometrical configuration of a transpiration test set-up can be derived from transpiration experiments using model liquids with known properties such as water or acetone. For transpiration evaporation experiments with a fully developed laminar gas flow (even with obstacles), existing Sherwood relations [2] can be used to predict the convective mass transport of volatile species into a carrier gas. The presence of a boat disturbs the gas flow profile and consequently the existing, from literature derived Sherwood relations for mass transfer of evaporation species, need to be adapted.

For a more complex geometrical configuration of a transpiration test set-up, CFD modelling appears to be a useful tool to predict the mass transport of volatile species into a carrier gas and to understand the fluid dynamics in the gas phase and distribution of volatile species in this phase. Results of the CFD-modelling for water evaporation tests at room temperature have been validated by transpiration experiments. Excellent agreement was found between model results and experiments as the difference between the experimental measured evaporation rates and the CFD modelling results are less than 2%.

In a partly filled rectangular boat with a rim above the water surface level, the results of CFD-modelling show recirculation loops in the tube above the liquid. This recirculation will influence the local Sherwood number. The results of CFD modelling and of simple water transpiration evaporation experiments at room temperature can be used to obtain relatively simple mass transport relations (Sh as a function of Re and Sc) for a fixed geometry of the transpiration test set-up. These relations were shown to be applicable for other evaporating liquids as well.

From the results of water transpiration measurements in a transpiration set-up at room temperature, the evaporation rates of water at higher temperatures (about 47 °C) were predicted as well as the acetone evaporation rates at room temperature. In both cases the average error in the predicted evaporation rates is less than 5%. This method was successfully validated in the range from $5 < Re < 1000$.

This paper presents mass transport equations in the gas phase for transpiration evaporation experiments in tubes. By the use of transpiration tests missing data for equilibrium vapour pressures (p_i^*) of liquids and melts (for instance salt, metal or glass melts) can be derived.

Acknowledgements

The authors to thank John Simon (Borax), Wibo Roolvink (PPG), Fabrice Fasilow (Glaverbel) and Peter Vrabel (Rona Crystal) for their support and contribution to this project.

References

[1] U. Merten, W.E. Bell, Transpiration method, in: J.L. Margrave (Ed.), The Characterization of High Temperature Vapors, Wiley, New York, London, Sidney, 1967, pp. 91–114.
[2] Verein Deutscher Ingenieure, Chapter G: Wärmeübertragung bei erzwungener einphasiger Strömung, in VDI-Wärmeatlas, 6th ed., VDI-Verlag GmbH Düsseldorf (1991), ISBN 3-18-401084-8.
[3] R.G.C. Beerkens, J.A.C. van Limpt, Evaporation in industrial glass melt furnaces, Int. J. Glass Sci. Technol. 74 (9) (2001) 245–257.
[4] R.G.C. Beerkens, Modelling the kinetics of volatilization from glass melts, J. Am. Ceram. Soc. 84 (9) (2001) 1952–1960.
[5] R. Conradt, H. Scholze, Zur verdampfung aus glasschmelzen, Glastechn. Ber. 59 (2) (1986) 34–52.
[6] M. Cable, M.H.V. Fernandes, Volatilisation of molten sodium metaborate with convection of the furnace atmosphere, Phys. Chem. Glass. 39 (4) (1998) 228–235.
[7] D.M. Sanders, H.A. Schaeffer, Reactive vaporization of soda-lime-silica glass melts, J. Am. Ceram. Soc. 59 (3–4) (1976) 96–101.
[8] H.A. Schaeffer, D.M. Sanders, Verdampfungsvorgänge an einem Na_2O–CaO–SiO_2–Glas, Dampfdruck- und Konzentrationsprofilmessungen, Glastech. Ber. 49 (5) (1976) 95–102.
[9] O. Knacke, O. Kubaschewski, K. Hesselman, Thermochemical Properties of Inorganic Substances, Springer-Verlag/Verlag Stahleisen, 1973, ISBN 3-540-54014-8, pp. 810–811.
[10] I. Barin, Thermochemical Data of Pure Substances, VCH Verlagsgesellschaft, 1989, ISBN 3-527-27812-5, pp. 265–266, pp. 649–650.
[11] R.C. Reid, J.M. Prausnitz, B.E. Poling, The Properties of Gases and Liquids, Fourth ed., McGraw-Hill Book Company, New York, 1987, ISBN 0-07-051799-1.

[12] R.B. Bird, W.E. Stewart, E.N. Lightfoot, Transport Phenomena, second ed., John Wiley & Sons, 2002, pp. 77-78, 420, 525–528.
[13] E.N. Fuller, J.C. Giddings, A comparison of methods for predicting gaseous diffusion coefficients, J. Gas Chromatogr. 3 (1965) 222.
[14] E.N. Fuller, K. Ensley, J.C. Giddings, Diffusion of halogenated hydrocarbons in helium. The effect of structure on collision cross-sections, J. Phys. Chem. 73 (1969) 3679–3685.
[15] E.N. Fuller, P.D. Schettler, J.C. Giddings, A new method for prediction of binary gas-phase diffusion coefficients, Ind. Eng. Chem. 58 (1966) 18–27.
[16] W.K. Lewis, W.G. Whitman, Principles of gas absorption, Ind. Eng. Chem. 16 (1924) 1215–1220.
[17] J.M. Smith, E. Stammers, L.P.B.M. Janssen, Fysische Transport Verschijnselen I, Delftse Uitgevers Maatschappij b.v., 2 ed. druk, 1981, pp. 146–148, ISBN 90-6562-050-8.
[18] K. Rietema, Fysische transport- en overdrachtsverschijnselen, Uitgeverij Het Spectrum, Utrecht/Antwerpen, 1976, pp. 118–119, 208–209.
[19] V. Gnielinski, Zur Waermeuebertragung bei laminarer Rohrstroemung und konstanter Wandtermperatur, Chem. Ing. Techn. Techn. 61 (2) (1989) 160–161.
[20] K. Stephan, Waermeuebergang und Druckabfall bei nicht ausgebildeter Laminarstroemung in Rohren und in ebenen Spalten, Chem. Ing. Techn. Techn. 31 (1959) 773–778.
[21] H. Martin, Vorlesung Wärmeübertragung II, Univ. Karlsruhe (TH), 1990.
[22] G.K. Batchelor, An Introduction to Fluid Dynamics, Cambridge University Press, 1970.
[23] J.H. Ferziger, M. Perić, Computational Methods for Fluid Dynamics, Springer, Berlin, 1999.
[24] S.V. Patankar, Numerical Heat Transfer and Fluid Flow, Hemisphere Publishing Co., McGraw-Hill, Washington, DC, New York, 1980.
[25] R.L. Verweij, Parallel computing for furnace simulations using domain decomposition, Ph.D. Thesis, Delft University of Technology, 1999.
[26] A. Twerda, Advanced computational methods for complex flow simulation, PhD thesis, Delft University of Technology, 2000.